Theory of electron energy spectrum and Aharonov-Bohm effect in self-assembled $In_xGa_{1-x}As$ quantum rings in GaAs

V. M. Fomin,* V. N. Gladilin,† S. N. Klimin,‡ and J. T. Devreese§
Theoretische Fysica van de Vaste Stoffen, Departement Fysica, Universiteit Antwerpen, Groenenborgerlaan 171, B-2020 Antwerpen, Belgium

N. A. J. M. Kleemans and P. M. Koenraad
Photonics and Semiconductor Nanophysics, COBRA, Eindhoven University of Technology, P.O. Box 513, NL-5600 MB Eindhoven, The Netherlands

(Received 20 July 2007; published 21 December 2007)

We analyze theoretically the electron energy spectrum and the magnetization of an electron in a strained $In_xGa_{1-x}As/GaAs$ self-assembled quantum ring (SAQR) with realistic parameters, determined from the cross-sectional scanning-tunneling microscopy characterization of that nanostructure. The SAQRs have an asymmetric indium-rich craterlike shape with a depression rather than an opening at the center. Although the real SAQR shape differs strongly from an idealized circular-symmetric open ring structure, the Aharonov-Bohm oscillations of the magnetization survive.

DOI: 10.1103/PhysRevB.76.235320 PACS number(s): 73.23.Ra, 71.15.−m, 73.21.La, 73.22.−f

I. INTRODUCTION

Electrons confined to a small ring manifest their quantum nature by an oscillatory behavior of their energy levels as a function of an applied magnetic field. This effect originates from the periodic dependence of the phase of the electron wave function on the magnetic flux through the ring, the Aharonov-Bohm effect,[1] and is usually associated with the occurrence of persistent currents in the ring.[2–5] The first experimental evidence of Aharonov-Bohm oscillations was found in metallic[6,7] and semiconductor[8] rings in the mesoscopic regime. In recent years, the fabrication and the investigation of $In_xGa_{1-x}As$ self-assembled quantum rings (SAQRs) have been rapidly progressing and led to a large number of experimental[9–14] and theoretical[15–18] studies.

SAQRs are formed by capping self-assembled quantum dots (QDs) grown using Stranski-Krastanov mode with a layer thinner than the dot height and by subsequent annealing.[9] During this process, anisotropic redistribution of the QD material takes place, resulting in elongated ring-shaped islands on the surface, with craterlike holes in their centers, as was shown with atomic force microscopy (AFM) topography measurements.[9] The dot-to-ring transition has been attributed to a dewetting process which expels the indium from the QD[19] and a simultaneous strongly temperature dependent Ga-In alloying process.[13]

Capacitance and far-infrared spectroscopy on SAQRs have provided evidence of an Aharonov-Bohm oscillation.[10] Measurements of the vertical Stark effect of excitons confined to individual SAQRs[12] have shown comparatively large electric dipole moments with sign opposite to that in quantum dots.[20] However, theoretical calculations have indicated that both the observed electronic radius and the dipole moment of the QRs are inconsistent with the geometry, as determined by AFM.[17]

This discrepancy has been resolved on the basis of the analysis of the shape, size, and composition of SAQRs at the atomic scale performed by cross-sectional scanning-tunneling microscopy (X-STM).[21,22] It has been found that AFM only shows the material coming out of the QDs during the QR formation. The remaining parts of the QDs, as observed by X-STM, possess indium-rich craterlike shapes that are actually responsible for the ringlike properties of SAQRs. These quantum craters do not have an opening at the center. The crucial question arose whether these singly connected anisotropic craterlike structures can effectively manifest the electronic properties (such as the Aharonov-Bohm oscillations) peculiar to the doubly connected geometry of the ideal rings.

Recently, the magnetic moment has been measured at low temperature on a sample consisting of 29 layers of SAQRs, designed such that each quantum ring confines one or two electrons. Using an ultrasensitive torsion magnetometer in magnetic fields up to 15 T, the oscillatory persistent current in SAQRs has been observed,[23] with a magnitude of oscillation as large as about 60%–70% of the corresponding magnitude in an ideal ring.

In the present paper, based on the structural information from the X-STM measurements, we calculate the electron energy spectra and the magnetization of a single-electron SAQR. The electron energy spectra and the magnetization of two-electron SAQRs will be analyzed elsewhere.[24] The paper is organized as follows. In Sec. II, a model of the SAQR is described. In Sec. III, the physical problem is formulated. In Sec. IV, the adiabatic potentials are presented and a solution is found for the in-plane electron motion. The effects of the shape anisotropy, strain, and temperature on the electron energy spectra and the magnetization in the SAQR are discussed in Sec. V. Section VI contains the conclusions.

II. MODEL

We model the SAQR structure with a varying-thickness $In_xGa_{1-x}As$ layer embedded in a infinite GaAs medium. The bottom of the $In_xGa_{1-x}As$ layer is considered to be perfectly flat and parallel to the xy plane. The height of the $In_xGa_{1-x}As$

 ©2007 The American Physical Society

layer as a function of the radial coordinate ρ and of the angular coordinate φ is modeled by the expression

$$h(\rho,\varphi) = h_0 + \frac{[\tilde{h}_M(\varphi) - h_0]\{1 - [\rho/\tilde{R}(\varphi) - 1]^2\}}{\{[\rho - \tilde{R}(\varphi)]/\tilde{\gamma}_0(\varphi)\}^2 + 1}, \quad \rho \leqslant \tilde{R}(\varphi),$$

$$h(\rho,\varphi) = h_\infty + \frac{\tilde{h}_M(\varphi) - h_\infty}{\{[\rho - \tilde{R}(\varphi)]/\tilde{\gamma}_\infty(\varphi)\}^2 + 1}, \quad \rho > \tilde{R}(\varphi), \quad (1)$$

with

$$\tilde{h}_M(\varphi) = h_M(1 + \xi_h \cos 2\varphi), \quad (2)$$

$$\tilde{\gamma}_0(\varphi) = \gamma_0(1 + \xi_\gamma \cos 2\varphi), \quad (3)$$

$$\tilde{\gamma}_\infty(\varphi) = \gamma_\infty(1 + \xi_\gamma \cos 2\varphi), \quad (4)$$

$$\tilde{R}(\varphi) = R(1 + \xi_R \cos 2\varphi). \quad (5)$$

Here, h_0 corresponds to the thickness at the center of the crater, h_M to the rim height, and h_∞ to the thickness of the $In_xGa_{1-x}As$ layer far away from the ringlike structure. The parameters γ_0 and γ_∞ define the inner and outer slopes of the rim, respectively. The parameters ξ_h, ξ_γ, ξ_R describe the anisotropy of the ring-shape.

A typical shape of a SAQR is shown in Fig. 1(a) for R =11.5 nm, h_0=1.6 nm, h_M=3.6 nm, h_∞=0.4 nm, γ_0=3 nm, γ_∞=5 nm, ξ_h=0.2, ξ_γ=0, and ξ_R=0. In the particular case when ξ_γ=0, ξ_R=0, Eq. (1) leads to the model considered in Refs. 21 and 22.

A three-dimensional finite-element calculation based on the elasticity theory is used to determine the relaxation of the cleaved surface of the modeled QR. With R=10.75 nm, h_0 =1.6 nm, h_M=3.6 nm, h_∞=0.4 nm, $\gamma_0=\gamma_\infty$=3 nm, ξ_h=0.2, ξ_γ=−0.25, and ξ_R=0.07, an indium concentration of 55% results in a calculated surface relaxation that matches the measured relaxation of the cleaved surface, as shown in Ref. 22. This set of geometric parameters of a SAQR is selected as the standard for the calculations discussed below, unless stated otherwise.

III. PROBLEM

The Hamiltonian of an electron in a strained ring takes the form[25,26]

$$H_e = -\frac{\hbar^2}{2}\left(\nabla - \frac{e}{\hbar}\mathbf{A}\right)\frac{1}{m_e(\mathbf{r}_e)}\left(\nabla - \frac{e}{\hbar}\mathbf{A}\right) + U_e(\mathbf{r}_e) + \delta E_e(\mathbf{r}_e) - eV_P(\mathbf{r}_e), \quad (6)$$

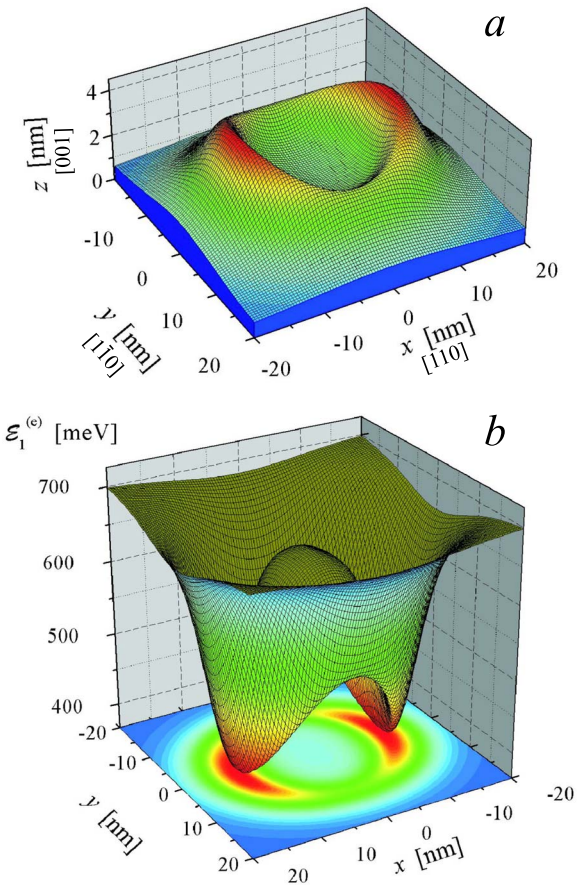

FIG. 1. (Color online) (a) Height of a SAQR as a function of the radial and the azimuthal coordinates as modeled by the function (1). (b) The adiabatic potential governing the electron motion in a SAQR shown in panel (a).

where $m_e(\mathbf{r}_e)$ is the electron band mass and $\mathbf{A}=\mathbf{e}_\varphi H\rho/2$ is the vector potential of the uniform magnetic field $\mathbf{H}=\mathbf{e}_z H$. $U_e(\mathbf{r}_e)$ is the conduction band edge, determined by the In content x, in the absence of strain. The strain-induced shift of the conduction band,

$$\delta E_e = a_e(\varepsilon_{xx} + \varepsilon_{yy} + \varepsilon_{zz}) \quad (7)$$

depends on the hydrostatic component of the strain tensor ε_{jk}.

The shear strains give rise to the piezoelectric potential

$$V_P(\mathbf{r}) = -\frac{1}{4\pi\varepsilon_0\varepsilon_r}\int \frac{\operatorname{div}\mathbf{P}}{|\mathbf{r}-\mathbf{r}'|}d^3\mathbf{r}', \quad (8)$$

determined by the piezoelectric polarization $P_i=e_{ijk}\varepsilon_{jk}$, where for InAs and GaAs only the piezoelectric moduli $e_{123}=e_{213}=e_{312}$ differ from zero; ε_r is the relative dielectric constant. The relevant material parameters are e_{123}^{InAs} =0.045 C/m^2, e_{123}^{GaAs}=0.16 C/m^2,[26] a_e^{InAs}=−5.08 eV, and a_e^{GaAs}=−7.17 eV.[27] The electron band mass as well as the parameters e_{123} and a_e for $In_xGa_{1-x}As$ are taken from a linear interpolation between the corresponding values for InAs and GaAs.

The components of the strain tensor ε_{jk} as well as the distribution of indium x for the revealed geometry of a SAQR were calculated following a three-dimensional finite-element method of the elasticity theory. Using the tables of ε_{jk} and x, we first numerically calculate and tabulate the distributions of the strain-induced shifts of the band edges [Eq. (7)] and of the piezoelectric potential [Eq. (8)].

Then, the Schrödinger equation,

$$H_e\Psi^{(e)}(\mathbf{r}) = E\Psi^{(e)}(\mathbf{r}), \tag{9}$$

is solved within the adiabatic approximation, using the *ansatz*

$$\Psi^{(e)}(\mathbf{r}) = \psi_k^{(e)}(z;\rho,\varphi)\Phi_{kj}^{(e)}(\rho,\varphi), \tag{10}$$

where the index k numbers subbands due to the size quantization along the z axis,

$$\left[-\frac{\hbar^2}{2}\frac{\partial}{\partial z}\frac{1}{m_e(\rho,\varphi,z)}\frac{\partial}{\partial z} + V_e(\rho,\varphi,z) + \delta E_e(\rho,\varphi,z) - eV_P(\rho,\varphi,z)\right]\psi_k^{(e)}(z;\rho,\varphi) = \mathcal{E}_k^{(e)}(\rho,\varphi)\psi_k^{(e)}(z;\rho,\varphi). \tag{11}$$

The Schrödinger equation [Eq. (11)] for the "fast" degree of freedom (along the z axis) is solved numerically for each node of a two-dimensional grid in the (ρ,φ) plane. As a result, we obtain the adiabatic potentials $\mathcal{E}_k^{(e)}(\rho,\varphi)$, tabulated on the aforementioned grid.

IV. ADIABATIC POTENTIALS: SOLUTIONS FOR THE IN-PLANE MOTION

A SAQR—although it reveals a potential hill near its axis—is a singly connected structure. It is then not evident whether or not its electronic states resemble those in a doubly connected (ideal ringlike) geometry. Such a resemblance can be expected if the central maximum of the adiabatic potential [shown, e.g., in Fig. 1(b) for the SAQR model represented in Fig. 1(a)] is sufficiently high. Moreover, the adiabatic potential possesses two pronounced minima, which can be regarded as the potential profile of two quantum dots. If the potential minima are sufficiently deep, the electron is localized in one of those quantum dots, and no persistent current occurs. When the depth of the potential minima is reduced, the electron tunneling between the potential minima of the adiabatic potential becomes more probable. If the potential minima are shallow enough, the electron can rotate around the center of the SAQR and persistent currents can occur.

Below, we represent the adiabatic potential $\mathcal{E}_1^{(e)}(\rho,\varphi)$, which corresponds to the lowest state of the size quantization along the z axis, using the indium distribution (see Fig. 2) and the strain data for a realistic SAQR as found using the finite-element numerical calculation package ABAQUS,[28] which is based on the elasticity theory. The solutions for the strain field on a grid lead to numerical noise in Figs. 2 and 3. We have checked that the noise does not affect the general conclusions of the present work.

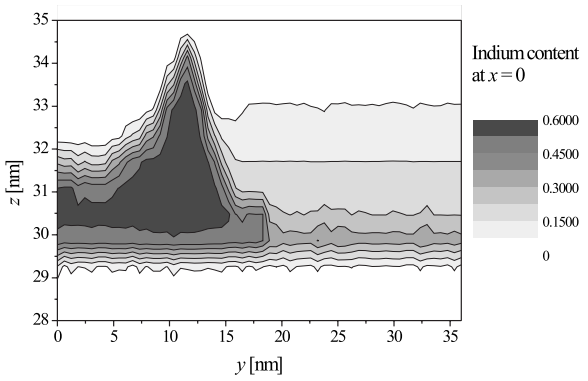

FIG. 2. Indium distribution in the yz plane in the SAQR.

In Fig. 3(a), the adiabatic potential $\mathcal{E}_1^{(e)}(\rho,\varphi)$, calculated in the absence of strain (i.e., taking into account only the indium distribution shown in Fig. 2), is shown as a function of the radial coordinate ρ for three different in-plane directions: along the x axis ($\varphi=0$), along the y axis ($\varphi=\pi/2$), and along the diagonal direction $x=y$ ($\varphi=\pi/4$). Along the y axis, the potential well for an electron is on average deeper and narrower compared to that along the x axis.

As seen from Fig. 3(b), where we plot the adiabatic potentials $\mathcal{E}_1^{(e)}$, due to strain, the depth of the potential well for an electron significantly decreases [compare panels (b) and (a) in Fig. 3]. The influence of the piezoelectric potential on the shape of the adiabatic potential $\mathcal{E}_1^{(e)}$ along the x and y axes is almost negligible. For the direction $x=y$, the effect of the piezoelectric potential on $\mathcal{E}_1^{(e)}$ is more pronounced but still does not seem to be crucial in determining the electron in-plane motion.

Recently, it has been shown[29] that including the piezoelectric potentials by calculating the induced charges to the first order in the shear strain tensor matrix elements actually overestimates the magnitude and may lead to a wrong sign of the piezoelectric potential in InAs/GaAs quantum dots. However, this would not change our conclusions for the SAQR under consideration because, as shown above, the piezoelectric correction for the adiabatic potential resulting from Eq. (8) with the polarization calculated to the first order in strain, even if overestimated, is nearly negligible.

The Schrödinger equations for the "slow" degrees of freedom,

$$\left[-\frac{\hbar^2}{2}\left(\nabla_{\rho,\varphi} - \frac{e}{\hbar}\mathbf{A}\right)\frac{1}{m_k^{(e)}(\rho,\varphi)}\left(\nabla_{\rho,\varphi} - \frac{e}{\hbar}\mathbf{A}\right) + \mathcal{E}_k^{(e)}(\rho,\varphi)\right] \times \Phi_{kj}^{(e)}(\rho,\varphi) = E_{kj}^{(e)}\Phi_{kj}^{(e)}(\rho,\varphi), \tag{12}$$

with the effective mass

$$m_k^{(e)}(\rho,\varphi) = \int dz|\psi_k^{(e)}(z;\rho,\varphi)|^2 m_e(\rho,\varphi,z), \tag{13}$$

determine the eigenstates of the in-plane motion, which are labeled by the index j. The Schrödinger equation [Eq. (12)] with an (anisotropic) adiabatic potential $\mathcal{E}_k^{(e)}(\rho,\varphi)$ and position-dependent effective mass $m_k^{(e)}(\rho,\varphi)$ cannot be solved analytically.

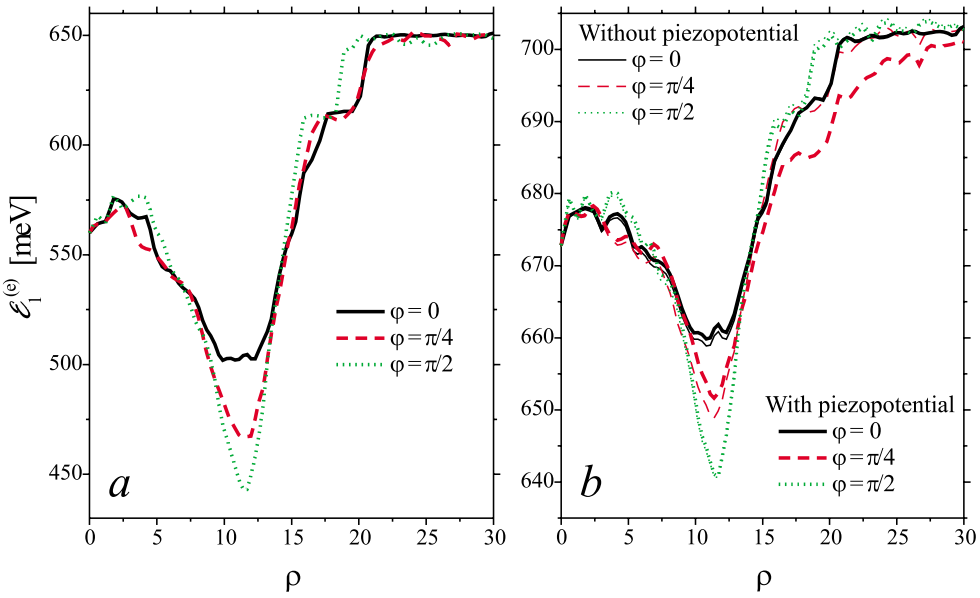

FIG. 3. (Color online) Adiabatic potential, calculated in the absence (a) and in the presence (b) of strain, as a function of the radial coordinate ρ for three different in-plane directions, determined by the angular coordinate φ. In panel (b), heavy (thin) curves are obtained with (without) the piezoelectric potential.

We find the eigenstates of the in-plane motion by numerical diagonalization of the Hamiltonian, which enters the left-hand side (lhs) of Eq. (12), in the basis of eigenfunctions of an auxiliary Hamiltonian with a constant effective mass $\bar{m}_k^{(e)}$ and a simplified adiabatic potential. We choose this simplified adiabatic potential in the form

$$\bar{\mathcal{E}}_k^{(e)}(\rho) = v_k^{(e)} + w_k^{(e)}\rho^2. \tag{14}$$

Since the potential [Eq. (14)] is isotropic, the corresponding in-plane eigenfunctions can be written as

$$\bar{\Phi}_{knL}^{(e)}(\rho,\varphi) = \bar{\chi}_{knL}^{(e)}(\rho)e^{iL\varphi}, \tag{15}$$

where n labels the radial solutions. Our basis wave functions [Eq. (15)] are the Fock-Darwin eigenfunctions[30–32] of a two-dimensional harmonic oscillator in a magnetic field, which were extensively used in the theory of quantum dots (see, e.g., Refs. 33–35 and references therein).

Inserting into Eq. (12) the adiabatic potential [Eq. (14)] instead of $\mathcal{E}_k^{(e)}(\rho)$, a constant effective mass $\bar{m}_k^{(e)}$, and wave functions in the form of Eq. (15), one obtains the one-dimensional Schrödinger equation

$$(\bar{\chi}_{knL}^{(e)})'' + \frac{1}{\rho}(\bar{\chi}_{knL}^{(e)})' + \left[\frac{2\bar{m}_k^{(e)}}{\hbar^2}(E_{knL}^{(e)} - v_k^{(e)}) + \frac{L}{l^2} - \frac{L^2}{\rho^2} - (\alpha_k^{(e)}\rho)^2\right]\bar{\chi}_{knL}^{(e)} = 0, \tag{16}$$

where $l = \sqrt{\hbar/(eH)}$ is the magnetic length and

$$\alpha_k^{(e)} = \sqrt{\frac{1}{4l^4} + \frac{2\bar{m}_k^{(e)}w_k^{(e)}}{\hbar^2}}. \tag{17}$$

The eigenfunctions of Eq. (16) are

$$\bar{\chi}_{knL}^{(e)}(\rho) = C_{knL}\rho^{|L|}\exp\left(-\frac{\alpha_k^{(e)}\rho^2}{2}\right)L_n^{(|L|)}(\alpha_k^{(e)}\rho^2),$$

$$n = 0,1,2,\ldots, \tag{18}$$

where $L_n^{(m)}(x)$ are generalized Laguerre polynomials and C_{knL} are normalization constants. The corresponding eigenenergies are

$$E_{knL}^{(e)} = v_k^{(e)} + \frac{\hbar^2}{\bar{m}_k^{(e)}}\left[\left(n + \frac{1}{2} - \frac{L}{2}\right)\frac{1}{l^2} + |L|\alpha_k^{(e)}\right]. \tag{19}$$

We are interested in the lowest energy states of an electron in the SAQR. Therefore, we restrict our calculations to the states in the lowest subband of the (strong) size quantization along the z axis (i.e., we consider states with $k=1$). For each value of the applied magnetic field, the electron eigenstates in the SAQR are found by numerical diagonalization of the adiabatic Hamiltonian, which enters the lhs of Eq. (12), in a finite basis of the in-plane wave functions $\bar{\Phi}_{1nL}^{(e)}(\rho,\varphi)$, given by Eq. (15) with the $\bar{\chi}_{1nL}^{(e)}(\rho)$ of Eq. (18). This finite basis includes functions with $n=0,\ldots,n_{max}$ and $L=-L_{max},\ldots,L_{max}$. In our calculations, we use $n_{max}=15$ and $L_{max}=12$. The parameters of the auxiliary Hamiltonian are taken as $v_1^{(e)}=650$ meV, $w_1^{(e)}=0.43$ meV/nm^2, and $\bar{m}_1^{(e)}=0.053m_0$.

As a result, we obtain the energies, $E_{1j}^{(e)}$, and the wave functions,

$$\Psi_{1j}^{(e)}(\mathbf{r}) = \psi_1^{(e)}(z;\rho,\varphi) \sum_{L=-L_{max}}^{L_{max}} \chi_{1jL}^{(e)}(\rho) e^{iL\varphi}, \tag{20}$$

of the lowest single-electron states in the SAQR as a function of the applied magnetic field. Here,

$$\chi_{1jL}^{(e)}(\rho) = \sum_{n=0}^{n_{max}} a_{1jnL} \bar{\chi}_{1nL}^{(e)}(\rho). \tag{21}$$

The index $j=1,2,3,\ldots$ labels states in order of increasing energy.

V. RESULTS

A. Shape anisotropy effect

The effect of the ring-height anisotropy, described by the parameter ξ_h, on the oscillations of the calculated electron magnetic moment μ, induced by the persistent current, as a function of magnetic field H has been studied in Ref. 22. The electron magnetic moment at zero temperature,

$$\mu = -\mu_B \frac{\partial E_1^{(e)}}{\partial H}, \tag{22}$$

is calculated numerically via the ground state energy $E_1^{(e)}$ of an electron in the SAQR; μ_B is the Bohr magneton.

Shape anisotropy of the SAQR results in a *mixing* of electron states with different magnetic quantum numbers. The transition magnetic fields, which correspond to sharp jumps of μ due to the interchange between the ground and first excited electron energy levels, increase with increasing ξ_h. Variations of the rim height $\tilde{h}_M(\varphi)$ with φ suppress oscillations of μ versus H. The effect of variations of the rim width with φ on $\mu(H)$ is qualitatively the same as that due to variations of $\tilde{h}_M(\varphi)$: for sufficiently large ξ_γ, the oscillating behavior of $\mu(H)$ is strongly suppressed.

In Fig. 4, we compare the magnetic moment $\mu(H)$ [Eq. (22)], calculated for SAQRs with nonzero ξ_h and ξ_γ of opposite sign, with the results for a perfectly symmetric ring and for a ring with relatively large variations of the rim height and a uniform rim width. As implied by Fig. 4, well-pronounced oscillations of $\mu(H)$ can be expected even for SAQRs with a strong shape anisotropy, provided that the width of the rim changes as a function of φ in *antiphase* with the rim height. Remarkably, this condition is satisfied for realistic SAQRs as characterized by X-STM[21] [see also Fig. 3(b)], where the parameters ξ_h and ξ_γ have opposite sign, so that the height and the width of the rim vary with φ in such a way that the effects of these variations on the cross-sectional area of the rim (in the ρz plane) partially compensate each other.

B. Strain effect

In Fig. 5, the lowest electron energy levels, calculated with and without effects due to strain, are shown as a function of the applied magnetic field H. Since the potential well for an electron in the strained SAQR is relatively shallow [see Fig. 3(b)], there exist only few discrete energy levels

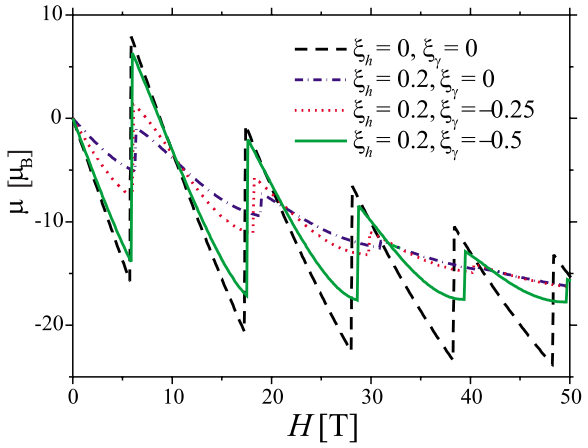

FIG. 4. (Color online) Magnetic moment induced by the ground-state persistent current as a function of the applied magnetic field for $In_{0.6}Ga_{0.4}As$ SAQRs with $R=10.75$ nm, $h_0=1.6$ nm, $h_M=3.6$ nm, $\gamma_0=3$ nm, and $\xi_R=0$ at different values of the anisotropy parameters ξ_h and ξ_γ.

below the continuum of states in the GaAs barrier. Due to the reduced potential barrier at the center of a strained ring, the effective electron radius *decreases* when taking into account strain. Correspondingly, the transition magnetic fields, where the ground and first excited electron energy levels inter-

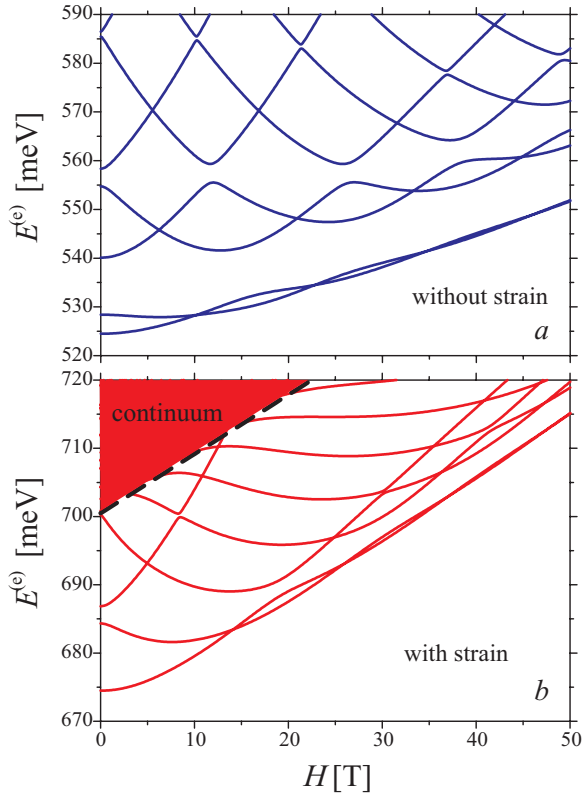

FIG. 5. (Color online) Electron energy spectra in a SAQR, calculated without (a) and with (b) effects due to strain. Energies are counted from the bottom of the conduction band in unstrained InAs. A dashed line, indicating the region of the continuum as obtained from our numerical simulation, is a guide to the eyes.

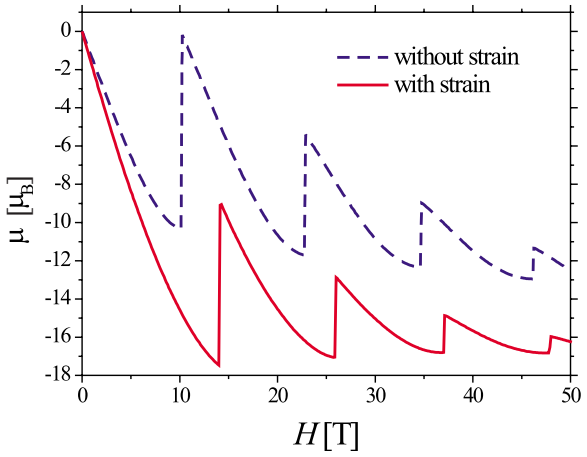

FIG. 6. (Color online) Ground-state magnetic moment of an electron in a SAQR, calculated with (solid curve) and without (dashed curve) effects due to strain.

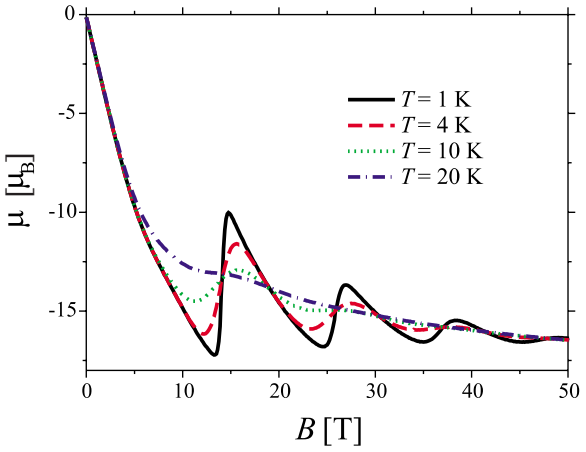

FIG. 7. (Color online) Calculated magnetic moment of an electron in a SAQR as a function of the applied magnetic field at various temperatures.

change, are *higher* in a strained ring than in an unstrained one (see Fig. 5).

As we have shown above, strain-induced effects reduce the magnitude of the variations of the adiabatic potential as a function of the azimuthal angle. As a result, at low magnetic fields, *the mixing of electron states with different magnetic quantum numbers, which occurs due to the shape anisotropy of a SAQR, is weakened in a strained ring*, as compared to the case when strain is absent. The consequences of the weakening of state mixing are clearly seen in Fig. 5. At $H < 10$ T, the energy spacing between the lowest electron state (which arises from the state with $L=0$ in a circularly symmetric ring) and the first excited state (which arises from the state with $L=-1$ in a circularly symmetric ring) is strongly enhanced due to strain. Also, the zero-field splitting between the first and second excited states (which correspond, respectively, to $L=-1$ and $L=1$ in a circularly symmetric ring) is significantly reduced when taking into account the strain-induced effects.

In Fig. 6, we plot the calculated ground-state magnetic moment of an electron, μ, as a function of the applied magnetic field. As seen from Fig. 6, the main effect of strain on the behavior of μ versus H is a shift of the transition fields toward higher H. This shift, already noticed when discussing the electron energy spectra, appears because strain leads to a *more shallow* potential well in the rim. When decreasing the depth of this potential well, the electron states tend to those in a flat disk. Correspondingly, strain effects also lead to an overall shift of the curve $\mu(H)$ (at nonzero H) toward larger negative values.

Figure 6 shows that oscillation amplitudes for $\mu(H)$ are not significantly influenced by strain. In fact, there occur two competitive effects of strain on the above oscillation amplitudes. On the one hand, due to the strain-induced reduction of the potential-well depth, there is an increasing penetration of the electron wave function into the barriers. This means an increase of the effective width of the ring. Such an increase of the ring width tends to *decrease the oscillation amplitude*. On the other hand, as mentioned above, the strain-induced reduction of the potential-well depth weakens the influence of shape anisotropy on the electron states. Correspondingly, the *suppression effect of shape anisotropy* on the oscillations of μ versus H *is weakened*, too.

C. Temperature effect

Here, we consider the temperature dependence of the Aharonov-Bohm oscillations in SAQRs. For arbitrary temperature T, the magnetic moment of an electron in an applied magnetic field H is calculated as

$$\mu = -\frac{\mu_B}{Z}\sum_{\tilde{n}} \exp\left(-\frac{E_{\tilde{n}}^{(e)}}{k_B T}\right)\frac{\partial E_{\tilde{n}}^{(e)}}{\partial H}, \tag{23}$$

where the index $\tilde{n}$ labels the energy levels $E_{\tilde{n}}^{(e)}$ of an electron in a SAQR and

$$Z = \sum_{\tilde{n}} \exp\left(-\frac{E_{\tilde{n}}^{(e)}}{k_B T}\right). \tag{24}$$

Calculations of μ were performed for a SAQR, using the electron energy spectra displayed in Fig. 5(b), taking into account strain. In Fig. 7, the calculated magnetic moment μ of an electron in a SAQR is shown as a function of the applied magnetic field at different temperatures. As seen from Fig. 7, an increase of T tends to smooth out the Aharonov-Bohm oscillations of $\mu(H)$. The smoothing effect is stronger at higher magnetic fields. Note that the suppression of the first Aharonov-Bohm oscillations (at relatively low H) is not dramatic for liquid He temperatures.

As implied by our results, for the SAQRs under consideration, the first magnetization jump, related to the Aharonov-Bohm effect, appears at magnetic fields ~14 T. In the experiment on SAQRs,[23] appreciable oscillations of the magnetization are detected just in this region of magnetic fields at $T=4.2$ K and $T=1.2$ K. A detailed comparison with the experimental data,[23] taking into account the dispersion of the geometric parameters of the SAQRs in the statistical ensemble, will be performed elsewhere.

VI. CONCLUSIONS

Based on the structural information from the X-STM measurements, we calculated the magnetization as a function of the applied magnetic field in SAQRs. Well-pronounced oscillations of the magnetization are expected even for SAQRs with a strong shape anisotropy because the rim width fluctuates as a function of the azimuthal angle in opposite phase with the rim height.

Our calculations indicate that in realistic $In_xGa_{1-x}As/GaAs$ SAQRs, the oscillatory behavior of the electron magnetic moment persists at relatively low magnetic fields $H<20$ T for temperatures below 10 K. Even though the SAQRs are singly connected and exhibit a pronounced shape anisotropy, they still show a magnetization behavior characteristic of an ideal-ring geometry that allows the observation of interference patterns revealing the quantum nature of electrons.

ACKNOWLEDGMENTS

We thank P. Offermans for performing some of the numerical calculations of the strain field. We acknowledge our collaboration with J. M. García, D. Granados, A. G. Taboada, J. H. Blokland, I. M. A. Bominaar-Silkens, P. C. M. Christianen, J. C. Maan, and U. Zeitler. This work was supported by the FWO-V Project Nos. G.0274.01N and G.0435.03, the WOG WO.035.04N (Belgium), and the EC Network of Excellence SANDiE, Contract No. NMP4-CT-2004-500101.

*Also at Photonics and Semiconductor Nanophysics, COBRA, Eindhoven University of Technology, P.O. Box 513, 5600 MB Eindhoven, The Netherlands and Physics of Multilayer Structures, Department of Theoretical Physics, State University of Moldova, A. Mateevici 60, MD-2009 Chişinău, Moldova.

†Also at Physics of Multilayer Structures, Department of Theoretical Physics, State University of Moldova, A. Mateevici 60, MD-2009 Chişinău, Moldova and Vaste-Stoffysica en Magnetisme Katholieke Universiteit Leuven, Celestijnenlaan 200 D, B-3001 Leuven, Belgium.

‡Also at Physics of Multilayer Structures, Department of Theoretical Physics, State University of Moldova, A. Mateevici 60, MD-2009 Chişinău, Moldova.

§Also at Photonics and Semiconductor Nanophysics, COBRA, Eindhoven University of Technology, P.O. Box 513, 5600 MB Eindhoven, The Netherlands.

[1] Y. Aharonov and D. Bohm, Phys. Rev. **115**, 485 (1959).
[2] N. Byers and C. N. Yang, Phys. Rev. Lett. **7**, 46 (1961).
[3] F. Bloch, Phys. Rev. B **2**, 109 (1970).
[4] M. Büttiker, Y. Imry, and R. Landauer, Phys. Lett. **96A**, 365 (1983).
[5] L. Wendler, V. M. Fomin, and A. A. Krokhin, Phys. Rev. B **50**, 4642 (1994).
[6] L. P. Lévy, G. Dolan, J. Dunsmuir, and H. Bouchiat, Phys. Rev. Lett. **64**, 2074 (1990).
[7] V. Chandrasekhar, R. A. Webb, M. J. Brady, M. B. Ketchen, W. J. Gallagher, and A. Kleinsasser, Phys. Rev. Lett. **67**, 3578 (1991).
[8] D. Mailly, C. Chapelier, and A. Benoit, Phys. Rev. Lett. **70**, 2020 (1993).
[9] J. M. García, G. Medeiros-Ribeiro, K. Schmidt, T. Ngo, J. L. Feng, A. Lorke, J. Kotthaus, and P. M. Petroff, Appl. Phys. Lett. **71**, 2014 (1997).
[10] A. Lorke, R. J. Luyken, A. O. Govorov, J. P. Kotthaus, J. M. García, and P. M. Petroff, Phys. Rev. Lett. **84**, 2223 (2000).
[11] R. J. Warburton, C. Schäflein, D. Haft, F. Bickel, A. Lorke, K. Karrai, J. M. García, W. Schoenfeld, and P. M. Petroff, Nature (London) **405**, 926 (2000).
[12] R. J. Warburton, C. Schulhauser, D. Haft, C. Schäflein, K. Karrai, J. M. García, W. Schoenfeld, and P. M. Petroff, Phys. Rev. B **65**, 113303 (2002).
[13] D. Granados and J. M. García, Appl. Phys. Lett. **82**, 2401 (2003).
[14] T. Raz, D. Ritter, and G. Bahir, Appl. Phys. Lett. **82**, 1706 (2003).
[15] A. O. Govorov, S. E. Ulloa, K. Karrai, and R. J. Warburton, Phys. Rev. B **66**, 081309(R) (2002).
[16] M. Bayer, M. Korkusinski, P. Hawrylak, T. Gutbrod, M. Michel, and A. Forchel, Phys. Rev. Lett. **90**, 186801 (2003).
[17] J. A. Barker, R. J. Warburton, and E. P. O'Reilly, Phys. Rev. B **69**, 035327 (2004).
[18] S. Viefers, P. Koskinen, P. S. Deo, and M. Manninen, Physica E (Amsterdam) **21**, 1 (2004).
[19] R. Blossey and A. Lorke, Phys. Rev. E **65**, 021603 (2002).
[20] P. W. Fry, I. E. Itskevich, D. J. Mowbray, M. S. Skolnick, J. J. Finley, J. A. Barker, E. P. O'Reilly, L. R. Wilson, I. A. Larkin, P. A. Maksym, M. Hopkinson, M. Al-Khafaji, J. P. R. David, A. G. Cullis, G. Hill, and J. C. Clark, Phys. Rev. Lett. **84**, 733 (2000).
[21] P. Offermans, P. M. Koenraad, J. H. Wolter, D. Granados, J. M. García, V. M. Fomin, V. N. Gladilin, and J. T. Devreese, Appl. Phys. Lett. **87**, 131902 (2005).
[22] P. Offermans, P. M. Koenraad, J. H. Wolter, D. Granados, J. M. García, V. M. Fomin, V. N. Gladilin, and J. T. Devreese, Physica E (Amsterdam) **32**, 41 (2006).
[23] N. A. J. M. Kleemans, I. M. A. Bominaar-Silkens, V. M. Fomin, V. N. Gladilin, D. Granados, A. G. Taboada, J. M. García, P. Offermans, U. Zeitler, P. C. M. Christianen, J. C. Maan, J. T. Devreese, J. H. Wolter, and P. M. Koenraad, in *Physics of Semiconductors*, edited by W. Jantsch and F. Schäffler, AIP Conf. Proc. No. 893 (American Institute of Physics, Melville, NY, 2007), pp. 683–684.
[24] V. M. Fomin, V. N. Gladilin, J. T. Devreese, N. A. J. M. Kleemans, and P. M. Koenraad (unpublished).
[25] J. A. Barker and E. P. O'Reilly, Phys. Rev. B **61**, 13840 (2000).
[26] M. Grundmann, O. Stier, and D. Bimberg, Phys. Rev. B **52**, 11969 (1995).
[27] C. G. Van de Walle, Phys. Rev. B **39**, 1871 (1989).
[28] http://www.simulia.com/products/abaqus_fea.html
[29] G. Bester, A. Zunger, X. Wu, and D. Vanderbilt, Phys. Rev. B **74**, 081305(R) (2006).
[30] V. Fock, Z. Phys. **47**, 446 (1928).
[31] C. G. Darwin, Proc. Cambridge Philos. Soc. **27**, 86 (1930).

[32] R. B. Dingle, Proc. R. Soc. London, Ser. A **211**, 500 (1952).
[33] L. Jacak, P. Hawrilyak, and A. Wójs, *Quantum Dots* (Springer, Berlin, 1998).
[34] D. Bimberg, M. Grundmann, and N. N. Ledentsov, *Quantum Dot Heterostructures* (Wiley, Chichester, 1999).
[35] T. Chakraborty, *Quantum Dots: A Survey of the Properties of Artificial Atoms* (Elsevier, Amsterdam, 1999).